Illustrating multipath propagation by means of sound waves

Luis Mendo *

August 2009

Abstract

A method is presented that uses sound waves to illustrate multipath propagation concepts. This is based on the existing analogy between radio and sound waves, and has the advantage that the required equipment is easily available. Different measurement techniques are introduced to respectively examine time dispersion, time variation, and both aspects of the multipath channel simultaneously. The proposed techniques are justified, example results are given, and the specific features that are illustrated by each type of measurement are discussed. Suggestions are given regarding application in courses on wireless communications.

Keywords: Communication engineering education; multipath channels; fading channels; dispersive channels; time-varying channels

1 Introduction

Educators of electrical engineering courses teach concepts for which concrete examples are often difficult to give. In particular, the theory of electromagnetic fields and radio wave propagation is based on ideas that the students may find difficult to grasp. Real-life examples are not abundant, and remain as somewhat unfamiliar constructions, as radio waves are not directly detected by our senses. The fact that the light wavelengths are so small implies that in our daily experience with light we do not normally detect effects such as diffraction or destructive interference, which, nevertheless, are very important in radio propagation. Therefore analogies with light, rather than help, can be detrimental, making the referred effects appear as counterintuitive.

---

*Computer Engineering Department, Autonomous University of Madrid; and Signals, Systems and Radiocommunications Department, Polytechnic University of Madrid. E-mail: lmendo@grc.ssr.upm.es

One of the fundamental aspects of radio communication is *multipath propagation*. Understanding this issue requires modelling the propagation channel as a linear time-variant system, characterized by its lowpass equivalent time-dependent impulse response. Throughout the paper, given a carrier frequency f_0, a bandpass signal will be denoted as $\tilde{x}(t)$, and its lowpass equivalent signal as $x(t)$, that is

$$\tilde{x}(t) = \text{Re}[x(t)e^{j2\pi f_0 t}].$$

Let $\tilde{s}(t)$ and $\tilde{r}(t)$ respectively denote the transmitted and received bandpass signals, with lowpass equivalent signals $s(t)$ and $r(t)$. The time-dependent impulse response of the lowpass equivalent channel, $h(t, \tau)$, is defined by the relationship

$$r(t) = \int_{-\infty}^{\infty} s(t - \tau)h(t, \tau)d\tau. \tag{1}$$

The time-dependent impulse response is difficult to visualize, because of the existence of *two* time variables.

To achieve a thorough understanding of multipath, it is important to have the possibility of "seeing" the propagation channel at work, i.e. transmitting a signal and observing the received signal. Although this can be accomplished using adequate radio equipment, the availability of such equipment may be limited because of its cost.

This paper proposes a simple and inexpensive method to visualize the different aspects of multipath propagation, using sound in stead of radio waves. This is based on the fact that radio propagation has many characteristics in common with that of sound waves; in particular, the existence of multipath. It should be noted that an exact characterization of a given propagation channel is not necessary (nor is it particularly enlightening); rather, the interest is in "aggregate" results, related to the general properties of the channel. Although the exact characterization (impulse response) of radio and sound propagation channels in the same environment will normally differ, the general properties are analogous in both cases.

The general idea of the measurements is to transmit a known signal, observe the received signal, and compare both to extract information about the lowpass equivalent channel response $h(t, \tau)$. The reception is carried out using a matched filter or correlator, which maximizes the received signal to noise ratio in the presence of additive white Gaussian noise [1, sec. 5.1]. Different choices of the transmitted signal allow observing different aspects of the impulse response; namely, the time-dispersion characteristics of the channel, related to the variable τ in $h(t, \tau)$, or the time-varying behaviour, which corresponds to the variable t.

The necessary equipment is described in Section 2. The experiments will be organized into three sections: time-dispersion measurements (Section 3), time-variation measurements (Section 4), and simultaneous time-dispersion

and time-variation measurements (Section 5). Suggestions on the application in a course on wireless communications are given in Section 6. Conclusions are summarized in Section 7.

Although all the techniques to be described can provide amplitude and phase information, only the former will be considered, i.e. $|h(t, \tau)|$, as this is deemed to be sufficiently descriptive while simplifying representation.

2   Equipment

The transmitted signal is generated in a computer and sent to a loudspeaker. The received signal is recorded by another computer using a microphone. It is recommended that two different computers are used, as many sound cards have a non-negligible electrical coupling from output to input. If the measurement is done with only one computer, the impulse response will contain an artificial peak caused by this coupling.

At the transmitter, an external, amplified loudspeaker is preferred, as built-in loudspeakers tend to have a poor response at low frequencies. Inexpensive, computer-oriented speakers are perfectly adequate. Since a pair of loudspeakers is normally used, the two of them should be placed together, or the balance control should be set so that only one produces sound. Signal generation and receiver processing can be carried out with Matlab or similar software. In the following it is assumed that Matlab is used. Transmission power is usually not an issue, as most amplified speakers are capable of delivering more sound power than is required for the measurements.

For the receiver, an external microphone is preferable, as this facilitates its displacement during the measurement. An inexpensive microphone, such as those intended for general computer use, is sufficient. Either omnidirectional or directional microphones may be employed. Nonetheless, if a highly directional microphone is used, it should be taken into account when interpreting the measurement. The signal picked up by the microphone is recorded and saved to a sound file, using any audio recording program. The sound file is then read by Matlab for receiver processing.

All the operations to be described have been implemented by the author in Matlab. The programs are available upon request.

3   Time-dispersion measurement

The purpose of this measurement is to illustrate the time dispersion caused by the propagation channel. Aspects related to time variation are not considered, that is, the channel is assumed to be time-invariant. This requires

that the equipment and the objects in the environment remain still while the transmission is taking place.

The channel is characterized by a time-invariant impulse response $h(\tau)$, and (1) reduces to $r(t) = s(t) * h(\tau)$, where "$*$" denotes convolution. Time dispersion is thus described by $h(\tau)$. A less informative description can be given in terms of the *delay spread* of the channel [2, sec. 2.3.2].

It will be assumed that $h(\tau) = 0$ for $\tau < 0$ (causality) and for τ exceeding a certain value τ_{max}, which represents an upper bound on the delays introduced by the channel.

3.1   Signal structure and receiver principle

The reliability with which a signal can be detected against noise can be characterized by the ratio of signal energy, E_{s}, to noise power spectral density, N_0. The signal energy is expressed as PT, where P denotes received signal power and T is the integration time. In order to simultaneously achieve high resolution and good sensitivity, *pulse compression* techniques can be applied [3, sec. 11.5]. In particular, direct-sequence spread-spectrum (DS-SS) signals can be used. The lowpass equivalent transmitted signal is thus

$$s(t) = \sum_{i=i_{\mathrm{min}}}^{i_{\mathrm{max}}} S[i] g(t - iT_{\mathrm{c}}),$$

where $g(t)$ is the lowpass equivalent *chip pulse* and $S[i]$ is a complex *chip sequence*. In this model, i_{min} and i_{max} may be either finite or infinite. For simplicity, $g(t)$ is restricted to be a real function; and it is assumed to be zero outside $[0, T_{\mathrm{c}}]$, i.e. non-overlapping, time-limited chip pulses are considered. With this approach, sensitivity can be improved by using a long signal and a large integration time T, whereas resolution is determined by the chip duration T_{c}, provided that the chip sequence has adequate autocorrelation properties, namely, a large *side-lobe level* (SLL), defined as the ratio of autocorrelation value for zero lag to the maximum absolute value for nonzero lags.

Since only amplitude information is sought, the receiver should carry out a *noncoherent* correlation of the received signal. A natural approach is to use $i_{\mathrm{min}} = 0$, $i_{\mathrm{max}} = M - 1$, i.e. a chip sequence of finite length M, and correlate the received signal with the complete transmitted signal. The integration time T equals the duration of the transmitted signal, MT_{c}, and the ability to discriminate paths with different delays depends on the *aperiodic autocorrelation* of the transmitted sequence, as well as on T_{c}.

Another possible approach is to use a periodic transmitted signal, obtained from repetitions of a chip sequence of finite length M, and correlate the received signal with a single period of the transmitted signal. In practice, the periodic signal may be substituted by a cyclically extended version, with

4

$i_{\min} = -m_1$, $i_{\max} = M + m_2 - 1$, for m_1, m_2 suitably selected. The integration time T corresponds to the period MT_c, and it is the *periodic autocorrelation* of the sequence that determines performance.

The two approaches are analyzed in the Appendix. For the present case, a periodic (cyclically extended) design using an m-sequence is preferred. This implies that $\tau_{\max}$ should not exceed MT_c in order to avoid ambiguity, and that the representation needs to be windowed, with a window length of MT_c. See Sections A.2 and A.4 in the Appendix for the details.

A rectangular chip pulse will be used. Small values of T_c are desirable, in order to obtain good resolution, but the allowed values are limited by the available bandwidth. The usable band for audio transmission is assumed to be from a few hundreds of Hz to several kHz. These conservative values assure that the frequency response in the transmitting and receiving equipment is reasonably flat. According to this, the carrier frequency is limited to a few kHz, and signal bandwidth should not exceed a value of the order of 1 kHz. Larger bandwidths can be used at the expense of some degradation in the measurement, as the "narrowband" assumption $f_0 \gg 1/T_c$ (see Section A.1 in the Appendix) gradually fails to hold. With these constraints, $f_0 \approx$ 3–3.5 kHz and $T_c \approx$ 0.7–1.5 ms appear as reasonable choices. Given that sound propagates at a speed $V \approx 340$ m/s in air, the selected T_c values correspond to path differences of 25–50 cm.

3.2 Receiver processing details

Since the operations are performed on a computer, integration is substituted by summation of discrete-time, quantized signals. Sample rates f_s of 44.1 or 48 kHz, which are standard values in digital audio [4, sec. 4.5], are sufficient. Quantization noise is not an issue with modern sound cards, which use at least 16 bits per sample.

The receiver computes the noncoherent correlation $z(\tau)$ from the bandpass received signal $\tilde{r}(t)$ (see Section A.2 in the Appendix), using (3) and (5). However, even though correlation is the optimum operation from the point of view of resulting signal to noise ratio, certain additional processing can be applied to improve other aspects of the estimation.

If the received signal $\tilde{r}(t)$ contains a strong interference or noise at a certain frequency f_i, the squaring operations involved in computing $z(\tau)$ may give rise to intermodulation products with f_0. In particular, a 50 or 60 Hz component, arising from mains electricity, is usually present, and may cause a visible ripple in $z(\tau)$, with a frequency close to f_0. To avoid this, it is convenient to filter the signal prior to the noncoherent correlation. The corresponding filter will be referred to as pre-filter. A discrete-time Butterworth design of order 4 and passband $[f_0 - 2T_c, f_0 + 2T_c]$ gives good results. Although this pre-filter hardly

Table 1. Restrictions on parameters for time-dispersion measurement

Lowpass equivalent model	$f_0 \gg 1/T_c$
Available bandwidth	100 Hz $< f_0 <$ 10 kHz
Sample rate	$f_s \gg f_0$
Frequency correction	$\delta \ll 1/(MT_c f_0)$
Time-invariance of the channel	During $(M + m_1 + m_2)T_c$
Ambiguity in τ	$\tau_{max} < MT_c$
Resolution in τ	T_c
Cyclic extension	$m_1, m_2 > \tau_{max}/T_c$
Integration time	MT_c
SLL	M

affects the signal, an identical filter can be applied at the transmitter to ensure matched-filtering operation at the receiver.

Assuming that two separate computers are used (as recommended in Section 2), a difference between sound card clock rates at transmitter and receiver will exist. Discrepancies of 30–80 ppm have been measured by the author. This implies that the pattern signals generated at the receiver have a slightly different carrier frequency than the received signal (the chip rate is also affected, but to a lesser extent, as it is smaller than the carrier frequency). For $T_c \approx 1$ ms and $f_0 \approx 3$ kHz, an m-sequence of $M = 4095$ gives an integration time of roughly 4 s, or 12000 carrier cycles. With a clock rate difference of 50 ppm, this introduces a phase change of more than half a cycle during the integration time, which can severely degrade the autocorrelation properties.

To solve this, carrier recovery is necessary [1, sec. 6.1.2]. A simplified, non-real time form of recovery can be used, exploiting the fact that the whole received signal is available at the time of processing. The procedure consists in carrying out the correlation using different carrier frequencies, and selecting the frequency which yields the largest peak in $z(\tau)$, i.e. that which maximizes $\max_\tau z(\tau)$. Let the candidate frequencies be given as $(1 + k\delta)f_0$, $k \in \mathbb{Z}$, where δ is a relative step. The latter should be selected such that δf_0 gives an accumulated phase change equal to a small fraction of a cycle, that is, $MT_c \delta f_0 \ll 1$. If the integration time MT_c is small, a δ value of the order of the expected clock rate difference (tens of ppm) may already fulfil the stated condition; in this case, frequency correction is not necessary (nor would it be reliable).

Table 1 indicates the restrictions on signal and receiver parameters.

3.3   Outline of program

The described steps are summarized as follows.
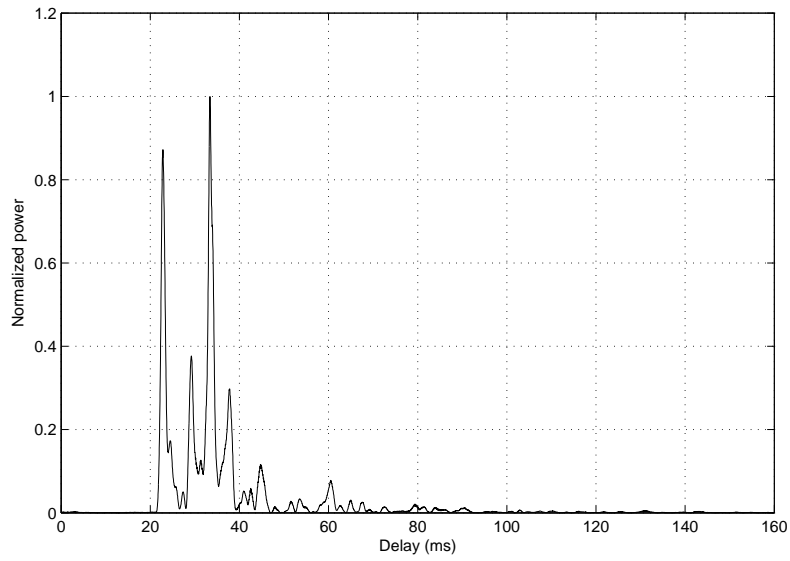
Time-dispersion measurement procedure

1. Transmitter:
   1.1. Generate $s(t)$ from m-sequence as in Section A.2, and obtain transmitted signal $\tilde{s}(t)$.
   1.2. Apply pre-filter to $\tilde{s}(t)$.
   1.3. Play signal.
2. Receiver:
   2.1. Record signal, save as sound file and read received signal $\tilde{r}(t)$ from file.
   2.2. Pre-filter signal.
   2.3. Generate correlation patterns $\tilde{s}_\mathrm{p}(t)$, $\tilde{s}'_\mathrm{p}(t)$ as defined in Section A.2, for different carrier frequencies within a given frequency span.
   2.4. Compute noncoherent correlation $z(\tau)$ from (3) and (5), for each receiver carrier frequency, and choose that which gives maximum peak.
   2.5. Plot windowed version of $z^2(\tau)$ as an estimation of $|h(\tau)|^2$.

3.4   Example results

The described procedure has been tested in a variety of environments. The results presented in this section, as well as those in subsequent sections, have been obtained with two laptop computers, using their internal sound cards. Consumer-range external loudspeakers and an inexpensive external microphone with moderate directivity have been employed.

Figure 1a displays the measured response in a laboratory room. The room size is $14 \times 8.5 \times 3$ m, and it is divided into three modules, with plenty of equipment and furniture. This gives a delay spread of the order of tens of ms. The measurement parameters are: $f_0 = 3.53$ kHz, $T_\mathrm{c} = 1.36$ ms, $f_\mathrm{s} = 44.1$ kHz, $M = 127$ and $m_1 = m_2 = 114$, with a maximum measurable delay $\tau_\mathrm{max} = 155$ ms. The condition for the frequency correction step is in this case $\delta \ll 1640$ ppm. Thus, taking into account that the clock rate difference is of the order of tens of ppm, frequency correction is not applied. The figure represents $|h(\tau)|^2$ normalized to a maximum value of 1. The observed graph is in accordance with the expected delay spread.

Figure 1b corresponds to a building lobby of size $17.5 \times 14 \times 6.5$ m, in which there are three columns and several decorative objects. Transmitter and receiver are located far apart, without line of sight. This constitutes a larger, more spacious environment, with a significant contribution from multiple reflections. The resulting channel is thus more dispersive, with delays of hundreds of ms, as can be seen in the figure. The signal parameters are the same as in Figure 1a, except that M is increased to 4095 to improve sensitivity and to allow detection of larger delays; and $m_1 = m_2$ are set as 1228, for a maximum measurable delay of 1.67 s. Frequency correction is necessary in

7

Figure 1a. Time-dispersion example measurement: indoor environment with moderate dispersion
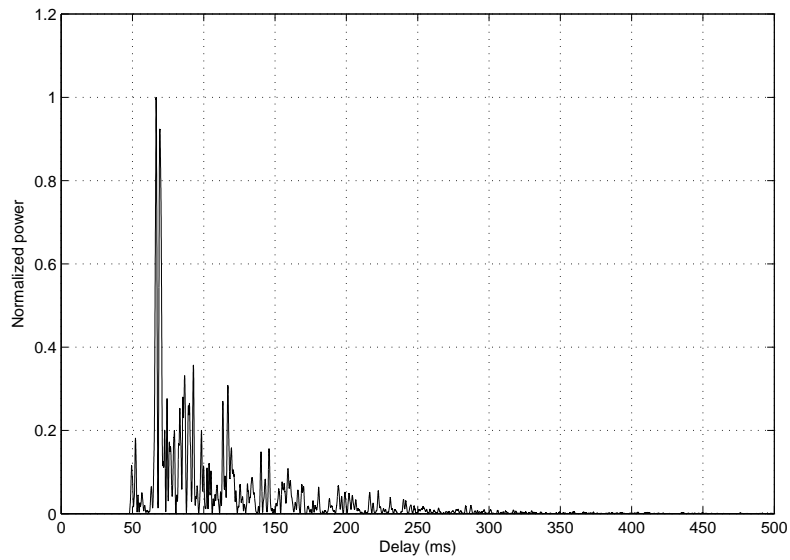
Figure 1b. Time-dispersion example measurement: building lobby with large dispersion

this case, with $\delta \ll 50$ ppm. A value $\delta = 5$ ppm is used.

3.5 Other features that can be observed with this measurement

The measurement primarily serves to illustrate the time-dispersion characteristics of the channel. The observed impulse response can be related to physical characteristics of the environment, such as room size, amount of furniture or existence of line of sight.

   As a by-product, the existence of clock drift can be employed to demonstrate the importance of carrier recovery in communication systems. If the sequence length is gradually increased without applying frequency correction, the noise is first reduced due to larger integration time, but above a certain length, when the accumulated phase error is a significant fraction of a cycle, the measurement sharply degrades.

4 Time-variation measurement

Time variation of the multipath channel manifests as fading, caused by constructive or destructive interference between different signal paths. The amount of time it takes for the fading level to change significantly is the *coherence time* of the channel.

   The time-variation aspect of the channel is best observed by transmitting a long signal with constant amplitude, i.e. a sinusoid, $\tilde{s}(t) = \cos(2\pi f_0 t)$, and representing the amplitude variations in the received signal. The lowpass equivalent transmitted signal is $s(t) = 1$, and thus (1) reduces to

$$r(t) = \int_{-\infty}^{\infty} h(t, \tau) d\tau.$$

This expression, in which the dependence on τ disappears by averaging, reflects the fact that time variations correspond to the t variable in $h(t, \tau)$.

   It will be assumed that the speed at which receiver, transmitter or any object in the environment move is bounded by a certain value $v_{\max}$.

4.1 Signal structure and receiver principle

Since the transmitted signal is a sinusoid, and only amplitude information is desired, the optimum strategy is again a noncoherent correlator or matched filter, which in this case is well approximated by a narrow bandpass filter tuned to f_0, followed by an envelope detector. This bandpass filter will be referred to as the receiving filter. Its output will be denoted as $\tilde{y}(t)$, and the output of the envelope detector as $z(t)$.

Table 2. Restrictions on parameters for time-variation measurement

Available bandwidth	$100 \text{ Hz} < f_0 < 10 \text{ kHz}$
Maximum displacement speed	$v_{\max} \ll V$
Sample rate	$f_{\text{s}} \gg f_0$
Receiving filter bandwidth	$B > 2f_0 v_{\max}/V$
Envelope detector cutoff frequency	$v_{\max}/V < f_{\text{e}}/f_0 \ll 1$
Integration time	$\approx 1/B$

The receiving filter helps remove noise and interference, and should be as narrow as possible. The received signal $\tilde{r}(t)$ has a nonzero bandwidth as a result of *Doppler spread* [1, sec. 14.1]. The maximum Doppler spread is $2v_{\max}/\lambda$ [5, sec. 3.2], where the wavelength λ is given as V/f_0. Thus the filter bandwidth B should be slightly larger than $2v_{\max}/\lambda$, in order to minimize noise while not altering the signal shape.

There is much freedom in the choice of f_0. Interestingly, values between 340 Hz and 3.4 kHz give wavelengths of 0.1–1 m, which in radio correspond to the ultra-high frequency (UHF) range.

4.2 Receiver processing details

The envelope detector can be realized by taking the absolute value of $\tilde{y}(t)$ and applying a lowpass filter, with cutoff frequency f_{e} much smaller than f_0, to remove the variations at the carrier frequency. An alternative would be to dispense with the envelope detector and represent $\tilde{y}(t)$; the envelope can be directly observed from the graph. In either case, in order to distinguish envelope variations from carrier variations, f_0 should be much greater than $v_{\max}/\lambda$, i.e. $v_{\max} \ll V$. This is clearly fulfilled with the displacement speeds occurring in practice. In the following it will be assumed that an envelope detector is used, and the obtained envelope will be plotted in dB.

The shape of the frequency response of the receiving filter is not very important, as long as it is approximately flat within the maximum Doppler spread. A Butterworth bandpass design of order 2, for example, gives good results. Carrier recovery is not needed, as the frequency variations due to clock rate differences are well within the filter bandwidth. For the lowpass filter of the envelope detector, a more selective frequency response is advised, such as that obtained with a Butterworth filter of order 4, in order to avoid visible ripples at f_0.

The restrictions on signal and receiver parameters are summarized in Table 2.

4.3 Outline of program

Time-variation measurement procedure
1. Transmitter:
    1.1. Generate transmitted signal (sinusoid), $\tilde{s}(t)$.
    1.2. Play signal.
2. Receiver:
    2.1. Record signal, save as sound file and read received signal $\tilde{r}(t)$ from file.
    2.2. Filter $\tilde{r}(t)$ to obtain $\tilde{y}(t)$.
   2.3. Obtain $z(t)$ as the envelope of $\tilde{y}(t)$.
    2.4. Plot $z(t)$.

4.4 Example results

Figure 2 shows measurements in an empty classroom of small size (capacity for 24 students). Two different carrier frequencies are used: $f_0 = 500$ Hz in Figure 2a and 2 kHz in Figure 2b, with a signal duration of 5 s. The sample rate is $f_s = 48$ kHz, and the receiving filter bandwidth is $0.02 f_0$. In both cases the microphone is moved at an approximate speed $v = 1$ m/s. This gives a Doppler spread of $2v/\lambda \approx 0.006 f_0$, which is within the filter passband. The cutoff frequency of the envelope detector is 50 Hz. Received power is normalized to its maximum value. It is seen that, even though the filter bandwidth is not tightly adjusted to that of the received signal, the filter removes a sufficient amount of noise to give an accurate representation up to the displayed 35-dB range; in fact, noise does not appear in the graph within the two small intervals before and after the signal is present, which indicates that it is below the -35 dB relative level.

In the figure, the length of the received signal is seen to be slightly greater than 5 s; this is due to time dispersion. The envelope variations have the typical aspect of multipath fading, with fades of more than 30 dB. The coherence time can be computed as the inverse of the Doppler spread, i.e. $\lambda/(2v)$. With $v = 1$ m/s, this gives 0.34 s for $f_0 = 500$ Hz and 0.085 s for $f_0 = 2000$ Hz, which is in agreement with the graphs.

4.5 Other features that can be observed with this measurement

The described measurement procedure is intended to illustrate time-varying fading, and the relationship between displacement speed, carrier frequency and coherence time. Additionally, frequency selectivity could be demonstrated by simultaneously transmitting at two different frequencies and comparing the results.
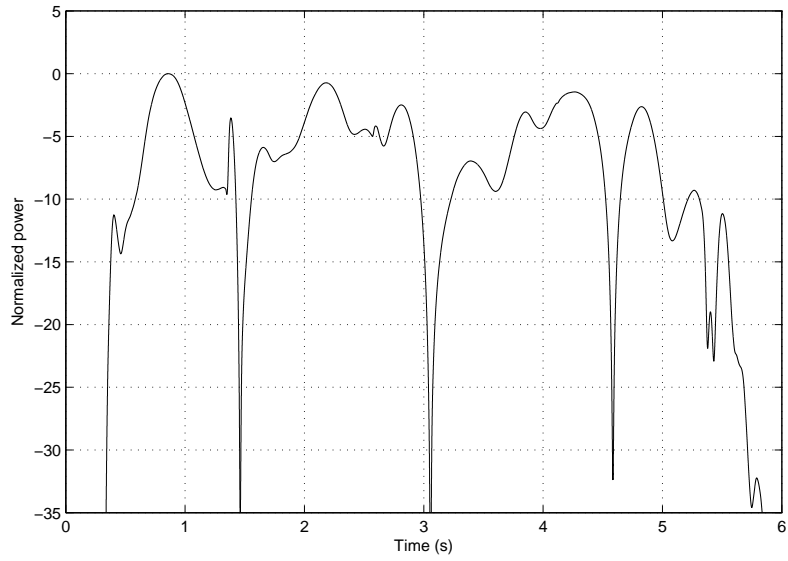
Figure 2a. Time-variation example measurement: carrier frequency
$f_0 = 500$ **Hz**
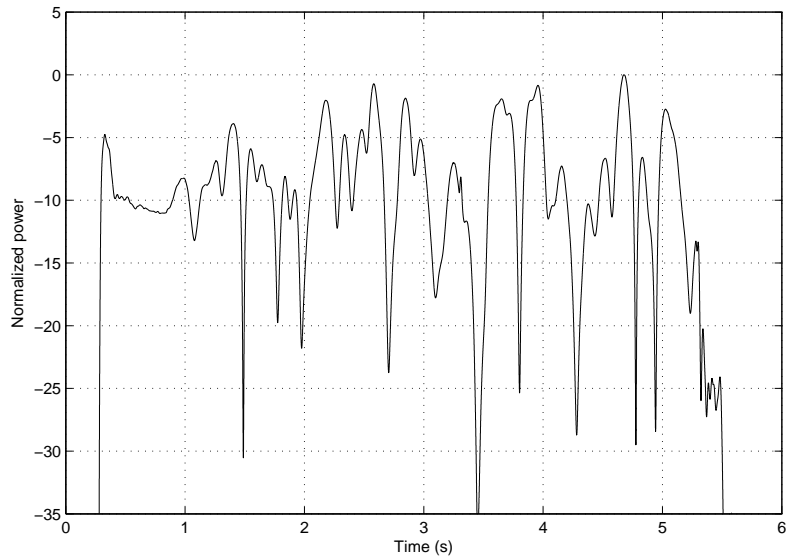
Figure 2b. Time-variation example measurement: carrier frequency
$f_0 = 2$ **kHz**

As a side issue, the measurement can illustrate noise removal in the received signal thanks to matched filtering. By using different receiving filter bandwidths, the improvement of signal to noise ratio can be made evident, with larger bandwidths resulting in noisier representations. This is best viewed by keeping the microphone and environment objects still, so that the signal envelope is constant. Note that this effect is particularly easy to observe here because, unlike in the time-dispersion measurement, the transmitted signal is a sinusoid, and the receiving operations do not alter its shape.

5 Simultaneous time-dispersion and time-variation measurement

While Sections 3 and 4 address the time-dispersion and time-variation aspects respectively, a complete characterization of the multipath channel requires dealing with both simultaneously, i.e. observing the full time-variant impulse response $h(t, \tau)$. As before, for the sake of simplifying representation, only its amplitude $|h(t, \tau)|$ will be considered.

As in previous sections, it will be assumed that $h(t, \tau) = 0$ for τ outside $[0, \tau_{\max}]$ and that movement speed does not exceed $v_{\max}$.

5.1 Signal structure and receiver principle

The measurement follows a similar procedure as in Section 3, only that repeated many times to capture time variation. Thus the lowpass equivalent transmitted signal $s(t)$ consists of a basic signal $s_{\mathrm{r}}(t)$ that is repeated R times with period T_{r}. It stems that an ambiguity equal to T_{r} is introduced in the measured delays. As detailed in Section A.5 in the Appendix, an aperiodic design, based on polyphase Barker sequences, is more suited to this measurement. This implies that $s_{\mathrm{r}}(t)$ consists of a short active part $s_{\mathrm{a}}(t)$ of duration $T_{\mathrm{a}} = MT_{\mathrm{c}}$, where M is the sequence length, followed by a gap of length $T_{\mathrm{r}} - T_{\mathrm{a}}$; and the integration time equals T_{a}. The value T_{a} must be chosen such that the channel is approximately invariant during this time; and T_{r} should be such that the channel variation is reasonably smooth during this period. The chip period and pulse shape are as in Section 3.1.

5.2 Receiver processing details

The receiver is similar to that described in Section 3.2, except that the effect of clock drift is different, and additional processing is needed to produce a graphical representation that includes time variation as well as time dispersion. This is discussed in the following.

Because the integration time is small, a correction of carrier frequency is not needed. However, since the measurement is repeated for a total time RT_r, the difference in clock rates may give a considerably large accumulated error in the measured delays. For example, if $RT_r = 20$ s, a 50 ppm difference gives a 1 ms error between delays measured at the beginning and at the end of the observation time; this error is of the order of T_c, and thus noticeable. To correct this, the received signal must be resampled. The adequate resampling ratio can be determined carrying out a long measurement of an invariant channel, and choosing the ratio which gives constant delays for the detected paths. An alternative, if the time-dispersion measurement has been previously performed, is to apply the same ratio as obtained for the carrier frequency in that case.

The function $|h(t,\tau)|^2$ is best displayed as an image, with the function value in dB represented by different colours or grey levels. In the following it will be assumed that t is represented on the horizontal axis, and τ on the vertical axis. The representation range for the function values should be slightly *smaller* than the SLL, so that most spurious peaks caused by secondary lobes are not shown. The reason is that, when a path is detected as an autocorrelation peak, all other paths produce interference through autocorrelation secondary lobes. The fact that these paths *simultaneously* interfere with the observed one gives rise to an interference level that may be above the SLL.

To compose the image, the domain of $z(\tau)$ is partitioned into intervals of length T_r, i.e.

$$[t_0 + iT_r, t_0 + (i+1)T_r), \quad i \in \mathbb{Z},$$

where t_0 is a time reference to be specified. This divides $z(\tau)$ into different segments $z_i(\tau)$, defined as

$$z_i(\tau) = z(\tau + t_0 + iT_r), \quad \tau \in [0, T_r).$$

Each segment is displayed as a vertical line in the image, with successive values of i corresponding to consecutive lines. The time reference t_0 should be chosen such that each of the measured responses $|h(t_i, \tau)|$ is contained in a vertical line of the image, i.e. it is not split between consecutive lines. The adjustment can be done automatically, exploiting the fact that, in most channels, received power tends to decrease with τ. Thus, $\max_\tau \sum_i z_i^2(\tau)$ is computed, and t_0 is set so that this maximum is located near the bottom of the image.

Another issue with the obtained image concerns its horizontal and vertical resolutions. The number of horizontal (t) pixels is R, whereas the number of vertical (τ) pixels is $T_r f_s$. The latter is typically much larger than can fit on a screen, and the former may be too small for adequate representation. This can be fixed by downsampling (with an anti-aliasing filter) in τ and upsampling (with interpolation) in t.

Table 3 summarizes the restrictions on signal and receiver parameters.

Table 3. Restrictions on parameters for simultaneous time-dispersion and time-variation measurement

Lowpass equivalent model	$f_0 \gg 1/T_c$
Available bandwidth	100 Hz $< f_0 <$ 10 kHz
Sample rate	$f_s \gg f_0$
Local time-invariance	$v_{max} \ll V/(f_0 M T_c)$
Time variation	$v_{max} \approx V/(f_0 T_r)$, or smaller
Resolution in t	T_r
Ambiguity in τ	$\tau_{max} < T_r$
Resolution in τ	T_c
Integration time	$M T_c$
SLL	M

5.3   Outline of program

Simultaneous time-dispersion and time-variation measurement procedure
1. Transmitter:
    1.1. Generate $s_a(t)$ and $s_r(t)$ from Barker sequence as in Section A.5. Obtain $s(t)$ and $\tilde{s}(t)$.
    1.2. Apply pre-filter to $\tilde{s}(t)$.
    1.3. Play signal.
2. Receiver:
    2.1. Record signal, save as sound file and read received signal $\tilde{r}(t)$ from file.
    2.2. Resample received signal.
    2.3. Pre-filter signal.
    2.4. Generate correlation patterns $\tilde{s}_a(t)$, $\tilde{s}'_a(t)$ from $s_a(t)$, as in Section A.1.
    2.5. Compute noncoherent correlation $z(\tau)$ as in (2) and (3), assuming equal received and transmitted carrier frequencies.
    2.6. Compose image, adjust horizontal and vertical resolutions and display.

5.4   Example results

It is recommended that the measurements are taken in environments with little or moderate time dispersion. A large τ_{max} requires a correspondingly large T_r, which in turn reduces v_{max}; thus too large delay spreads might require impractically slow movements. In addition, it is best to choose an environment that is not very cluttered. If there are many paths with similar delays, the representation becomes too "tangled", making it difficult to identify paths.

Figure 3 shows two measurements in the same indoor setting as in Figure 1a (laboratory room with low delay spread). Signal parameters are: $f_0 = 2.94$ kHz, $T_c = 0.68$ ms, $f_s = 44.1$ kHz, binary Barker sequence with $M = 13$,

15

$T_r = 113T_c = 77$ ms, $R = 180$. The selected T_c gives a delay resolution around 1 ms, and the signal length RT_r is 13.84 s. The origin of the vertical axis is arbitrary (as stems from Section 5.2). The represented $|h(t, \tau)|^2$ is normalized, with 0 dB corresponding to the maximum value.

In Figure 3a, all objects in the environment are stationary except that a metallic plate situated behind the microphone is initially still, then is slowly moved farther away, and then is still again. There is line of sight between transmitter and receiver. All resolvable paths are initially seen as horizontal lines, corresponding to constant delays, but at $t \approx 1.5$ s the delay of the second detected path begins to increase. This path corresponds to the wave reflected in the moving plate, while the first path is the direct ray, whose delay does not change. It is interesting to note how other paths also experience changes as a consequence of the plate moving. These paths correspond to multiple reflections involving the plate and other objects in the environment.

Consider the path with a single reflection in the moving plate. As its delay approaches that of some other path, both paths become indistinguishable for the correlator, and a characteristic interference pattern arises. This can be seen as a series of maxima and minima in the region where the lines described by the two paths cross. This phenomenon is evident in Figure 3a for $t \approx 6.5$–8.5 s. Similar patterns between other paths with larger delays are discernible as well.

In Figure 3b, the microphone is in line of sight from the loudspeaker, and it is hanging from its cable, oscillating like a pendulum along the direction from the loudspeaker. This gives an approximately sinusoidal variation in the delay of the direct path, as well as in several reflected paths, as is clearly seen in the image.

The figures obtained from the measurements presented in Sections 3 and 4 can be considered as particular cases of the type of representation described here. Namely, a time-dispersion measurement such as those in Figure 1 corresponds to a vertical cut of the $|h(t, \tau)|^2$ image. Similarly, the time-varying fading observed in Figure 2 is actually an interference pattern between unresolvable paths, analogous to that observed in Figure 3a; the difference is that in the time-variation measurement no attempt is made to resolve any paths, and thus all of them interfere, giving a more irregular pattern.

Even though the measurement procedure just presented is a generalization of the preceding ones, this generalization must be understood as a *compromise*, as there is a trade-off involved: since more information is extracted from the received signal, the quality of this information is necessarily degraded. Specifically, the achievable E_s/N_0 and SLL are lower than in the measurements described in Section 3, as M is here limited by the fact that the channel needs to be constant during the integration time. Likewise, the representation is noisier and has poorer time resolution than those of Section 4. Consequently,
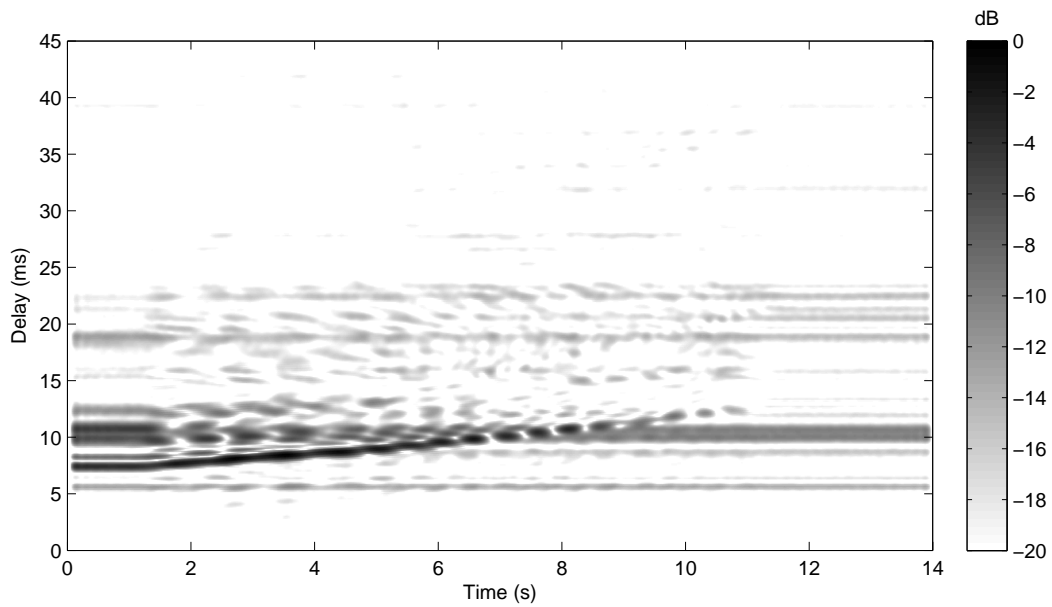
Figure 3a. Simultaneous time-dispersion and time-variation example measurement: reflecting object moving away from receiver
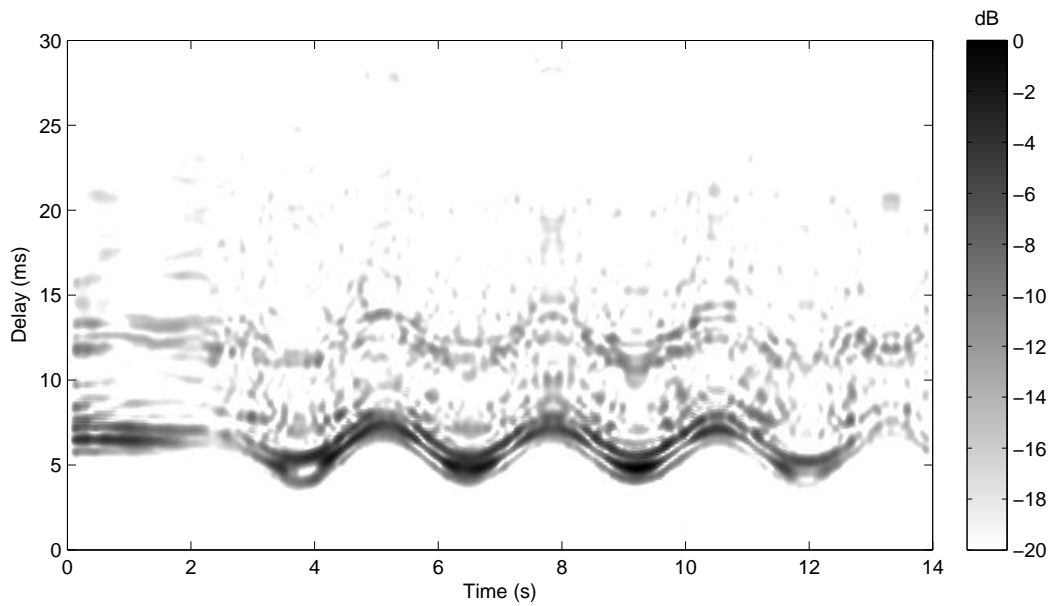
Figure 3b. Simultaneous time-dispersion and time-variation example measurement: receiver position oscillating along the direction from transmitter

the most appropriate type of measurement should be selected in each particular situation, depending on which aspects are deemed as more important.

5.5 Other features that can be observed with this measurement

Besides the time-dispersion and time-variation aspects, two other issues can be illustrated. Firstly, the existence of a clock rate difference can be made evident by carrying out the measurement in an invariant channel. For a sufficiently long measurement, the slope of the lines corresponding to the detected paths is apparent, and can be used to calculate the rate difference.

Secondly, the fact that the delay resolution is of the order of T_c is well known in the study of Rake receivers for DS-SS systems [1, sec. 14.5]. Two paths with a delay difference smaller than T_c are not resolved by the receiver, and thus interfere, causing fading. This can be vividly illustrated with this measurement, as seen in Figure 3a.

6 Application in a course on wireless communications

The described techniques can be applied in courses on wireless communications, either as laboratory work or as demonstrations performed by the teacher in the classroom. The former can bring greater student involvement, while the latter allows the teacher to more easily integrate measurements with exposition of the related theoretical content.

These measurement procedures have been used by the author in a course on mobile communications taught in the fifth year of the Telecommunication Engineering degree of the Autonomous University of Madrid. Two or three short classroom demonstrations are usually employed, interlaced with the theoretical content. The experience has proved fruitful and rewarding. Students' interest during the measurements is high, and they are happy to participate when invited; for example, by displacing the microphone, or by operating the transmitting computer while the teacher controls the receiver. Questions asked by the teacher are important for encouraging the students to interpret what they are seeing, focusing their attention towards the key aspects that can be observed.

The additional features illustrated by the measurements are useful for relating multipath propagation with concepts learned from digital transmission courses. This can broaden the vision of the subject and improve comprehension.

7 Conclusions

The use of sound waves to illustrate multipath propagation has been discussed. Three different techniques are proposed. The first characterizes time dispersion, while the second deals with time variation. The third described technique gives information on both aspects of the channel simultaneously, providing a full view of the time-variant impulse response, at the cost of reduced accuracy. In each case, the transmitted signal is suitably selected, and the receiver operations are discussed. Results are given that exemplify how the time-dispersion and time-variation aspects manifest in the measurements, and how they can be related to physical characteristics of the channel. Suggestions are given regarding application to courses on wireless communications.

A   Signal design for measuring the impulse response

This appendix discusses signal design for the estimation of the impulse response. The two approaches introduced in Section 3 for time-invariant channels are analyzed in Sections A.1 and A.2 respectively. The conditions on the transmitted signal that yield a good estimation are then derived in Section A.3. Based on this, the signal selection for a time-invariant channel is addressed in Section A.4. Finally, the design is extended to time-variant channels in Section A.5.

A.1   Design based on aperiodic autocorrelation

In the aperiodic design, $s(t)$ is expressed as

$$s(t) = \sum_{i=0}^{M-1} S[i]g(t - iT_\mathrm{C}),$$

where $S[i]$ is a sequence of finite length M, defined for $n = 0, \ldots, M-1$. The corresponding bandpass signal is

$$\tilde{s}(t) = \mathrm{Re}[s(t)e^{j2\pi f_0 t}],$$

and its quadrature phase shifted version is defined as

$$\tilde{s}'(t) = \mathrm{Re}[s(t)e^{j(2\pi f_0 t + \pi/2)}].$$

Let $\phi_x(\tau) = x^*(-\tau) * x(\tau)$ denote the autocorrelation function of a signal $x(t)$, and $\Phi_X[n] = X^*[-n] * X[n]$ the aperiodic autocorrelation of a finite-length sequence $X[n]$. From $\tilde{r}(t)$, the receiver can compute

$$y(\tau) = 2\tilde{s}(-\tau) * \tilde{r}(\tau), \quad y'(\tau) = 2\tilde{s}'(-\tau) * \tilde{r}(\tau). \tag{2}$$

Neglecting double-frequency terms, which is valid if $f_0 \gg 1/T_c$, i.e. if the bandpass signal is "narrowband" [1, sec. 4.1], it is easily seen that

$$y(\tau) = \text{Re}[h(\tau) * \phi_s^*(\tau)], \quad y'(\tau) = \text{Im}[h(\tau) * \phi_s^*(\tau)].$$

Therefore, defining

$$z(\tau) = \sqrt{y^2(\tau) + y'^2(\tau)}, \tag{3}$$

the following result is obtained:

$$z(\tau) = |h(\tau) * \phi_s^*(\tau)|. \tag{4}$$

A.2 Design based on periodic autocorrelation

In this case

$$s(t) = \sum_{i=-m_1}^{M+m_2-1} S[i \bmod M]g(t - iT_C),$$

where $S[i]$ is a sequence of finite length M. Initially, m_1 and m_2 are assumed to be ∞, i.e. $s(t)$ is periodic with period MT_c. Let $s_p(t)$ denote one period of $s(t)$, from $t = 0$ to MT_c, and let $\tilde{s}_p(t)$, $\tilde{s}'_p(t)$ be the corresponding in-phase and quadrature phase shifted bandpass signals. The receiver computes

$$y(\tau) = 2\tilde{s}_p(-\tau) * \tilde{r}(\tau), \quad y'(\tau) = 2\tilde{s}'_p(-\tau) * \tilde{r}(\tau). \tag{5}$$

Let $\psi_{s_p}(\tau) = s_p^*(-\tau) \circledast s_p(\tau)$, where "$\circledast$" denotes circular convolution. In the same conditions as in Section A.1, (5) gives

$$y(\tau) = \text{Re}[h(\tau) * \psi_{s_p}^*(\tau)], \quad y'(\tau) = \text{Im}[h(\tau) * \psi_{s_p}^*(\tau)].$$

Since $s(\tau)$ is periodic with period MT_c, so are $\psi_{s_p}(\tau)$, $y(\tau)$ and $y'(\tau)$. This has two implications. First, the measurement has a delay ambiguity of MT_c (this is analogous to range ambiguity in radar systems [3, sec. 1.1]). To avoid it, M should satisfy $M > \tau_{\max}/T_c$. Second, the receiver only needs to compute one period of $y(\tau)$ and $y'(\tau)$. This will be assumed to be the period extending from $\tau = 0$ to MT_c. As a result, the transmitted signal can be substituted by a finite-length version, i.e. m_1, m_2 can be finite. Thus $s(t)$, rather than being a periodic signal, becomes a "cyclic extension" of $s_p(t)$. Since $h(\tau)$ vanishes for $\tau \notin [0, \tau_{\max}]$, it is easily seen that for any finite $m_1, m_2 > \tau_{\max}/T_c$, the signals $y(\tau)$ and $y'(\tau)$ restricted to $\tau \in [0, MT_c]$ coincide with those obtained for infinite m_1, m_2. (It is seen that, compared with the aperiodic case, cyclically extending the signal transforms aperiodic correlation into periodic; this is analogous to the cyclic extension used in orthogonal frequency-division multiplexing, which transforms convolution into circular convolution [2, sec. 3.4.4].) Consequently, if m_1, m_2 satisfy the stated condition, and if $z(\tau)$ is defined as in (3) with τ restricted to the interval $[0, MT_c]$,

$$z(\tau) = |h(\tau) * \psi_{s_p}^*(\tau)|. \tag{6}$$

A.3 Conditions for good estimation

In view of (4) and (6), $z(\tau)$ can serve as an estimate of $|h(\tau)|$, $\tau \in [0, \tau_{\max}]$, both in the aperiodic and in the periodic case. The conditions for this estimation to be adequate are as follows. In the first case, since $h(\tau)$ appears after convolution with $\phi_s^*(\tau)$, the latter should resemble a narrow pulse. The function $\phi_s(\tau)$ can be expressed as

$$\phi_s(\tau) = \sum_{i=1}^{M-1} \sum_{j=1}^{M-1} S^*[i]S[j]\phi_g(\tau + (i-j)T_c),$$

from which

$$\phi_s(\tau) = \sum_{k=-M+1}^{M-1} \Phi_S[k]\phi_g(\tau + kT_c). \tag{7}$$

With the periodic approach, since $h(\tau)$ is convolved with the periodic function $\psi_{s_\mathrm{p}}^*(\tau)$, a period of the latter should resemble a narrow pulse. Defining the periodic autocorrelation of $S[i]$ as $\Psi_S[n] = S^*[-n] \circledast S[n]$, the function $\psi_s(\tau)$ is expressed as

$$\psi_{s_\mathrm{p}}(\tau) = \sum_{k=-\infty}^{\infty} \Psi_S[k]\phi_g(\tau + kT_c). \tag{8}$$

Therefore, in view of (7) or (8), two conditions have to be met for a good estimation:

(i) $\phi_g(\tau)$ should be very narrow. This function determines the shape and width of the main lobe of $\phi_s(\tau)$ or $\psi_{s_p}(\tau)$, and thus the delay resolution.

(ii) $\Phi_S[n]$ or $\Psi_S[n]$ should be approximately zero for $n \in \{1, \ldots, M-1\}$. This is achieved by an appropriate choice of the sequence $S[i]$. This condition affects the SLL of $\phi_s(\tau)$ or $\psi_{s_\mathrm{p}}(\tau)$.

Condition (i) basically reduces to selecting the smallest T_c compatible with bandwidth restrictions. As for condition (ii), with the aperiodic design, a convenient class of sequences is constituted by polyphase Barker sequences [6]. These have the form

$$S[i] = e^{j2\pi\theta_i/J}, \quad \theta_i \in \{0, 1, \ldots, J-1\}$$

for some $J \in \mathbb{N}$, and achieve the maximum possible SLL, equal to M, within all unit-modulus sequences. Polyphase Barker sequences are known up to $M = 63$ [7] [8], for values of J that tend to increase with M. Binary Barker sequences ($J = 2$) are known for several values of M up to 13.

Regarding periodic autocorrelation, m-sequences [1, p. 433] are optimum. These are binary sequences, which exist for $M = 2^m - 1$, $m \in \mathbb{N}$, and whose periodic autocorrelation $\Psi_S[n]$ equals -1 for $n \bmod M \neq 0$, resulting in an SLL $= M$.

A.4   Time-dispersion measurement

For the time-dispersion measurement, the periodic design based on m-sequences is preferred. The reason is that m-sequences exist for greater lengths M than polyphase Barker sequences, which gives larger SLL and E_s/N_0 in an invariant channel.

The noncoherent correlation $z(\tau)$, given by (6), is only useful for $\tau \in [0, MT_\mathrm{c}]$, as seen in Section A.2. Outside this interval, replicas of the central part are obtained as a result of the pattern signals $\tilde{s}_\mathrm{p}(t)$ and $\tilde{s}'_\mathrm{p}(t)$ in (5) partially matching the cyclic extensions present in $\tilde{r}(t)$. Thus the representation should be adequately windowed. (The replicas have amplitudes m_1/M and m_2/M times that of the central part respectively, and appear "noisier", as they have poorer autocorrelation properties.) The length of the window is MT_c, and its position can be manually adjusted.

A.5   Time-dispersion and time-variation measurement

A basic limitation in this case is that the channel must remain approximately invariant during the integration time; otherwise the received signal will be "transparent" to the correlator, as it will not match the pattern signals. Note that frequency correction, as applied in Section 3 to compensate clock rate differences, is not useful here, because frequency deviations caused by movement are much more severe than clock rate differences (for example, a radial velocity of 1 m/s produces a Doppler shift equal to 0.34% of the carrier frequency), and are not necessarily constant during the integration period.

The lowpass equivalent transmitted signal is

$$s(t) = \sum_{i=0}^{R-1} s_\mathrm{r}(t - iT_\mathrm{r}),$$

according to Section 5.1. If the periodic approach is used, $s_\mathrm{r}(t)$ is taken to be the signal $s_\mathrm{p}(t)$ defined in Section A.2, generated from an m-sequence, and the integration time equals T_r. Since a cyclic shift of an m-sequence is also an m-sequence [1, sec. 8.1.3], a resolution in t equal to T_c can be achieved, by correlating with different cyclic shifts of the sequence.

The problem with the periodic design is that T_r determines both the maximum unambiguous delay τ_max and the maximum speed v_max. Namely, the delay should satisfy $\tau_\mathrm{max} < T_\mathrm{r}$; and the condition that the channel remains approximately constant during T_r is $v_\mathrm{max} \ll V/(f_0 T_\mathrm{r})$. As a result, only channels with $v_\mathrm{max}\tau_\mathrm{max} \ll V/f_0$ can be measured. This condition is quite restrictive. As an example, for a moderate τ_max of 0.2 s and $f_0 = 3.4$ kHz, this gives $v_\mathrm{max} \ll 0.5$ m/s. Numerical experiments show that, for a binary sequence, an accumulated phase shift of $2\pi/3$ rad already causes noticeable degradation in

the autocorrelation. Thus, $v_{\max} < 0.17$ m/s in the example. The restriction could be alleviated by reducing f_0; however, this would degrade the delay resolution, because the chip rate must be significantly smaller than f_0, as seen in Section A.1.

The referred drawback can be avoided by means of a design based on aperiodic autocorrelation. The lowpass equivalent transmitted signal $s(t)$ is constructed from $s_r(t)$ as above; but now the repeated signal $s_r(t)$ has an active part $s_a(t)$ of length $T_a < T_r$, followed by a gap of length $T_r - T_a$. The correlation patterns $\tilde{s}_a(t)$, $\tilde{s}_a'(t)$ are obtained from $s_a(t)$ as in Section A.1. The integration time is T_a, and thus the maximum speed limitation is $v_{\max} \ll V/(f_0 T_a)$; whereas the delay restriction is $\tau_{\max} < T_r$ as before. Thus both limitations can be controlled independently. In exchange of this flexibility, the resolution in t is T_r instead of T_c, as the technique of correlating with different cyclic shifts cannot be applied here. This can be solved by interpolating in t, provided that the channel variation during T_r is reasonably smooth, i.e. that $v_{\max}$ is of the order of $V/(f_0 T_r)$ or smaller (note that this is a weaker condition than requiring that the channel be approximately constant during T_r). Otherwise, the interpolation will miss some of the channel variation, giving a smoothed, possibly aliased version.

For a signal $\tilde{s}_a(t)$ consisting of M chips, the described speed limitation determines the usable values of M. For example, taking $T_c = 1$ ms, $f_0 = 3$ kHz and $v_{\max} = 1$ m/s as typical values requires $M \ll 113$. In view of this, the fact that polyphase Barker sequences are known only for $M \leq 63$ is of no importance. In addition, numerical computation shows that the autocorrelation properties of these sequences are more sensitive to channel changes within T_a as the alphabet size J increases. Since, with currently known sequences, J grows rapidly with M (for example, $M > 15$ requires $J \geq 6$; see [6] and the references therein), the binary sequence of length $M = 13$ or the 6-phase sequence of $M = 18$ are seen as good choices, with SLL = 22.3 dB or 25.1 dB respectively. Of course, these small lengths give modest values of E_s/N_0; nevertheless, noise is well below autocorrelation secondary lobes for moderate volume levels at the transmitter.

Considering the above, the aperiodic design is chosen, with polyphase (or binary) Barker sequences of small lengths. The receiver computes $z(\tau)$ as in (2) and (3), except that $\tilde{s}(t)$, $\tilde{s}'(t)$ are replaced by $\tilde{s}_a(t)$, $\tilde{s}_a'(t)$. This gives a result analogous to that in Section A.1, only that repeated every T_r. Each repetition corresponds to a "snapshot" of the channel, i.e. an estimation of $|h(t_i, \tau)|$, $t_{i+1} = t_i + T_r$; and there is a delay ambiguity of T_r.

Acknowledgment

References

1. J. G. Proakis, *Digital Communications*, fourth edition, McGraw-Hill, 2001.

2. D. Tse and P. Viswanath, *Fundamentals of Wireless Communication*, Cambridge University Press, 2005.

3. M. I. Skolnik (editor), *Introduction to Radar Systems*, second edition, McGraw-Hill, 1980.

4. J. Watkinson, *The Art of Digital Audio*, third edition, Focal Press, 2001.

5. J. M. Hernando and F. Pérez-Fontán, *Introduction to Mobile Communications Engineering*, Artech House, 1999.

6. J. Jedwab, "What can be used instead of a Barker sequence?," *Contemporary Mathematics*, **461**, 2008, pp. 153–178.

7. P. Borwein and R. Ferguson, "Polyphase sequences with low autocorrelation," *IEEE Transactions on Information Theory*, **51**, 4, April 2005, pp. 1564–1567.

8. A. R. Brenner, "Polyphase Barker sequences up to length 45 with small alphabets," *Electronics Letters*, **34**, 16, August 1998, pp. 1576–1577.